RSC Mechanochemistry

Accepted Manuscript

This article can be cited before page numbers have been issued, to do this please use: F. Machado, R. M. M. Torresi and P. F. M. de Oliveira, *RSC Mechanochem.*, 2026, DOI: 10.1039/D6MR00004E.

View Article Online
DOI: 10.1039/D6MR00004E

Solid-to-Liquid Mechanochemistry: Multiscale Synthesis of Electrochemically Relevant Ionic Liquids

Felipe Machado, Roberto M. Torresi*, Paulo F. M. de Oliveira*

Institute of Chemistry, Fundamental Chemistry Department, University of São Paulo, Av. Prof. Lineu Prestes 748, 05508-000 São Paulo, Brazil.

* Corresponding author. E-mail address: rtorresi@iq.usp.br (R.M.T.), paulofmo@usp.br (P.F.M.O.)

Abstract: Ionic liquids (ILs) offer unique properties for electrochemical applications, but their synthesis typically requires large volumes of solvents and costly reagents, limiting scalability and sustainability. Here, we address this limitation by demonstrating a solvent-free mechanochemical route to five benchmark ILs of electrochemical relevance. The method enables the synthesis of both hydrophobic $Pyr_{14}TFSI$ (1-butyl-1-methylpyrrolidinium bis(trifluoromethanesulfonyl)imide) and hydrophilic $Pyr_{14}TfO$ (1-butyl-1-methylpyrrolidinium trifluoromethanesulfonate) ILs via solid-state metathesis reaction induced by mechanical mixing, requiring only minimal solvent for product recovery. This approach delivers high yields (> 80%) and nearly quantitative conversions (≥ 99%), producing ILs with low impurity levels. Additionally, we demonstrated the upscaling of the mechanochemical approach for the synthesis of $Pyr_{14}TFSI$ from 4 g to 99 g of reagents by transitioning from ball milling to a multi-shaft planetary mechanical mixer, achieving a 97% conversion in 30 minutes. These results underscore the mechanochemical potential for practical and sustainable production of ILs, establishing this approach as a rapid and efficient route for synthesizing both hydrophilic and hydrophobic ILs.

View Article Online
DOI: 10.1039/D6MR00004E

Introduction

Ionic liquids (ILs) are defined as salts with melting points below 100 ºC that are often liquids in ambient conditions. They are primarily composed of asymmetric ions: a bulky organic cation and an inorganic anion, allowing for an infinite number of possible combinations.[1–4] The appropriate cation/anion pairing is a key factor in determining the physicochemical properties of these compounds.[5] Typically, the most common cations found in commercial ILs of electrochemical interest are imidazolium, piperidinium, pyrrolidinium, ammonium, and phosphonium, while common anions include bis(trifluoromethanesulfonyl)imide ($TFSI^-$), bis(fluorosulfonyl)imide (FSI^-), triflate (TfO^-), hexafluorophosphate (PF_6^-), tetrafluoroborate (BF_4^-), dicyanamide (DCA^-), among others.[6,7] Their key properties include low vapor pressure, low flammability, high thermal stability over a wide temperature range, and excellent ion transport.[5,8] Due to their versatility and distinctive physicochemical properties, ILs have attracted considerable scientific attention over the decades. They have been used in a wide range of scientific applications, including the development of batteries[7,9,10] and supercapacitors[11,12], electrochemical sensors[13], organic catalysis[14], extraction[15] and many others.[16–19]

The most widely used ILs are predominantly synthesized in aqueous media, via metathesis reactions (i.e. ion exchange) due to the presumed simplicity and low cost of the method.[20,21] In general, an aqueous solution of an organic halide salt (e.g., Cl^-, Br^-, or I^-) containing the target cation is mixed with another aqueous solution of an alkali-metal (Li^+, Na^+, or K^+) or transition-metal (especially Ag^+) salt that supplies the desired anion. Depending on the nature of the cation/anion pair, the reaction produces a single aqueous phase for hydrophilic ILs, or two separate phases when the product is hydrophobic (**Figure 1A**). In the case of hydrophobic ILs, one phase consists essentially of the IL, while the second aqueous phase contains the residual salts in water (e.g., NaBr, KBr, KCl, etc.). These phases are then separated by extraction and/or distillation with an organic solvent, followed by purification. In contrast, for the case of hydrophilic ILs, a single phase remains after the reaction, containing the IL, water, and the halide salt byproduct. Because this byproduct is also water-soluble (if alkali-metal precursors are used), its removal introduces additional purification steps. For this reason, the synthesis of hydrophilic ILs often makes use of more expensive transition metal salts, which results in the formation of precipitates of the residual ions (e.g., AgBr, AgCl, or AgI). It is worth noting that, in both hydrophobic and hydrophilic systems, residual water and inorganic byproducts often remain as contaminants in the IL phase, unavoidably so for hydrophilic ILs.

View Article Online
DOI: 10.1039/D6MR00004E

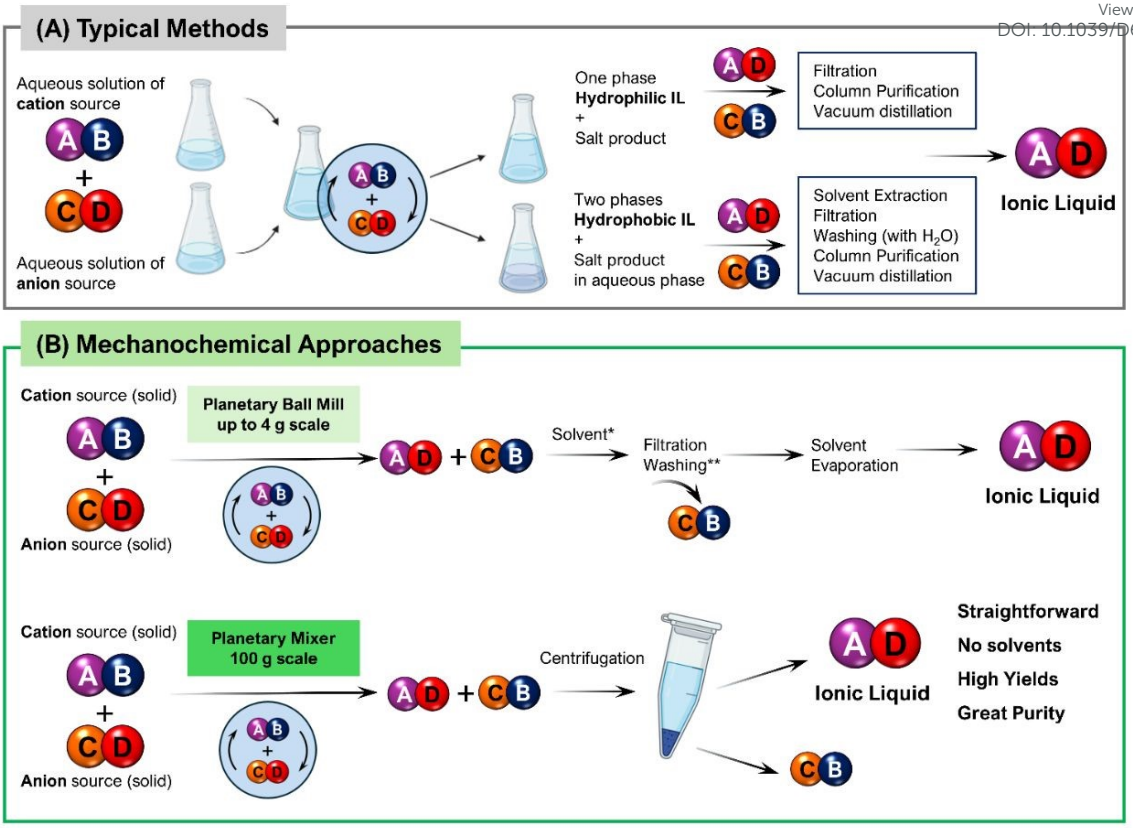

Figure 1. Flowchart comparing the traditional and mechanochemical methods for IL synthesis via ion exchange reaction.

Because of the phase behavior and purification needed as described above, achieving both high conversions and purity without extensive work-up remains a major challenge in the synthesis of ILs by metathesis reactions. The process still relies on large amounts of solvents, selected due to the limited and distinct solubility of reactants and products, as well as the extensive use of water. This results in lengthy separation steps and often still leaves significant residual halides, solvents, and water. It is well established in the literature that even small amounts of these residual components can significantly affect key properties such as viscosity, ionic conductivity, thermal stability, and the electrochemical window, which are detrimental to the IL performance, especially for electrochemical purposes.[22–28] Therefore, developing synthetic routes that minimize the work-up steps while resulting in ILs with tolerable levels of impurities is of significant interest. An alternative approach to reduce water use and avoid silver-based reagents for hydrophilic ILs has been proposed by Chen et al.[29]. In their study, $BMImBF_4$ was prepared from a saturated $NaBF_4$ aqueous solution. Although other methods are also reported in the literature[8] for the synthesis of ILs (e.g., alkylation[30], microwave-assisted[31], ultrasound-assisted synthesis[32], or chiral synthesis[33]), separation and purification procedures still require a large amount of solvent, or are limited to hydrophobic

View Article Online
DOI: 10.1039/D6MR00004E

systems.[34] Finally, the large-scale application of ILs remains significantly limited by their high cost, the challenges of scaling up production, and again, the purification steps.[35,36]

Here, we present the first effort to date that employs mechanochemical routes for ion-exchange reactions from solid precursors to synthesize both hydrophilic and hydrophobic ILs (**Figure 1B**), eliminating not only the use of water as a reaction solvent but also expensive transition metal salts (e.g., Ag^+ salts), especially for hydrophilic ILs. In addition, this study demonstrates a significant advance in producing ILs without using water and with reduced waste. In this paper, the ILs were selected based on their established relevance to electrochemical applications, particularly electrolytes in batteries, supercapacitors, and electrochemical cells. The ILs chosen were Pyr_{14}TFSI (1-butyl-1-methylpyrrolidinium bis(trifluoromethanesulfonyl)imide), Pyr_{14}FSI (1-butyl-1-methylpyrrolidinium bis(fluorosulfonyl)imide), Pyr14TfO (1-butyl-1-methylpyrrolidinium trifluoromethanesulfonate), Pip_{14}TFSI (1-Butyl-1-methylpiperidinium bis(trifluoromethaneylsulfonyl)imide), BDMImTFSI (1-butyl-2,3-dimethylimidazolium bis(trifluoromethanesulfonyl)imide).

With the advantage of mechanochemistry, which has emerged as a promising field for developing sustainable and faster solid-state synthetic routes driven by mechanical energy, new opportunities arise for more efficient chemical processes.[37–40] Mechanochemical routes have been widely used not only in the preparation of various chemical compounds and materials, including catalysts[41], organometallic compounds[42] and inorganic complexes[39], but also a variety of compounds prepared by ion exchange reactions[43]. Finally, it is worth noting that ILs have also been prepared mechanochemically by manual grinding, however, through a protonation/deprotonation of acidic or basic groups, generating ILs of pharmaceutical interest.[44,45] On the other hand, no studies have been found reporting the use of a mechanochemical route for the production of ILs from metathesis reactions, and addressing both the possibility of preparation of hydrophilic ILs without using water and the facilitated workup when producing ILs in larger amount.

Results and Discussion

We started the study with the most illustrative case, the hydrophilic IL Pyr_{14}TfO (1-butyl-1-methylpyrrolidinium-trifluoromethanesulfonate) (**Figure 2**). For the reaction, approximately 4 g of precursors in equimolar amounts were milled in a planetary ball mill (PBM) in a 45 mL Si_3N_4 milling set with 18 milling balls (ø = 10 mm, 1.16 g each) for

View Article Online
DOI: 10.1039/D6MR00004E

varying durations (30-240 min) and rotation speed (250-500 rpm) (Experimental details can be found in SI). The scheme of synthesis using PBM is displayed in **Figure 1B** (top).

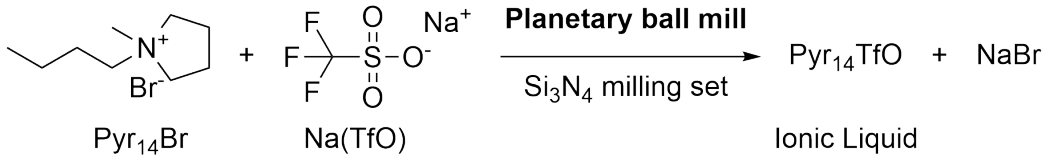

Figure 2. Scheme of ball mill synthesis of $Pyr_{14}TfO$ ionic liquid.

The product obtained after milling was a white suspension consisting of NaBr and the IL. To facilitate the recovery of the reaction mixture from the jar and to separate the IL from the formed NaBr, minimal amounts of dichloromethane (CH_2Cl_2) were used, 5.0 $mL_{solvent}\ g_{product}^{-1}$. It is important to clarify that the reaction occurs without any solvent. The latter is used only in subsequent steps, especially during separation stages. The suspension was then vacuum filtered to remove the sodium bromide, followed by solvent evaporation under reduced pressure (< 30 mbar at 60 °C). The resulting solid was analyzed by powder X-ray diffraction to check for any remaining precursors. The PXRD patterns of the solids obtained along with the ILs are shown in **Figure 3**.

Milling for 30 min at 250 rpm produced an X-ray amorphous solid. Increasing the milling time, however, led to the appearance of a crystalline phase. At first glance, the PXRD pattern after 60 min suggested that the $Pyr_{14}Br$ precursor was still present, mainly due to the peaks at 2θ = 22.3° and 23.4°. Nonetheless, a closer look at the possible phases involved in the system indicated that these Bragg peaks were from a hydrated phase of NaBr ($NaBr{\cdot}2H_2O$), which preferentially forms at shorter milling times at 250 rpm. $Pyr_{14}TfO$ precursors are highly hygroscopic, and the water in the NaBr hydrated phase likely originated from ambient humidity during manipulation before milling.

As the milling time increased, the expected cubic rock-salt structure of NaBr became dominant, being the major phase after 180 min. Raising the rotation speed from 250 to 500 rpm further promoted crystallization of the anhydrous NaBr cubic phase, although the hydrated form persisted. Although no signal of unreacted precursors was detected after 60 min, we decided to extend the milling for longer periods up to 240 min to ensure quantitative conversion, especially because the efficiency of the mechanical action under our conditions, presumably efficient for solids, is reduced by the presence of a relatively large liquid phase. In the final chosen conditions, the reaction reaches completion (> 99.9% conversion) with 93.4% yield after purification for $Pyr_{14}TfO$ IL.

View Article Online
DOI: 10.1039/D6MR00004E

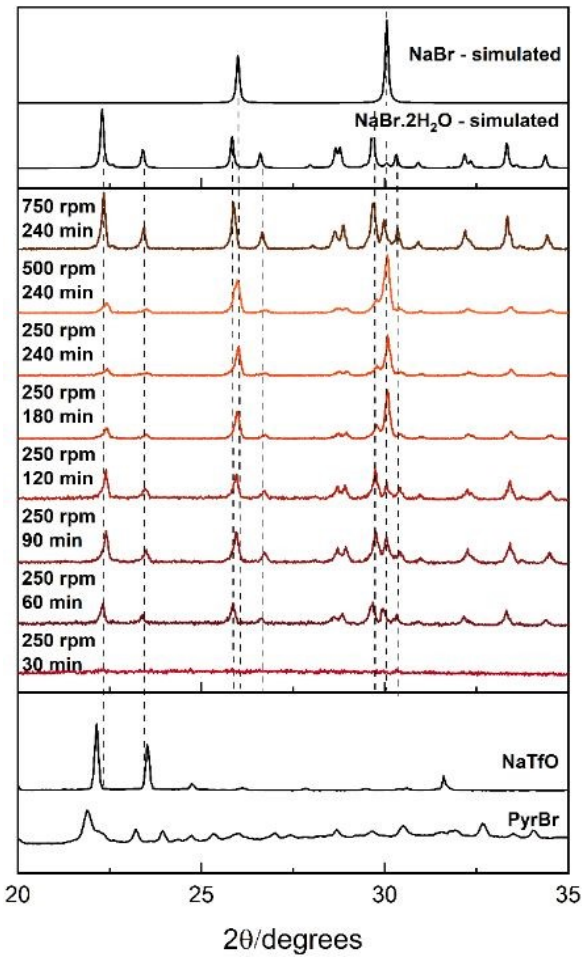

Figure 3. PXRD of the solid products formed during the milling-induced IL synthesis. The full pattern can be found in the ESI (**Figure S1**).

Given the similarity in reaction type and mechanism, the optimized conditions of 500 rpm and 240 minutes of milling used for $Pyr_{14}TfO$ synthesis were extended to the synthesis of all other ILs evaluated in this study (**Table 1**). This planetary milling approach (**Figure 1B – top**) enabled the successful synthesis of the other four ILs in quantitative conversions (Entries 2–5), which are hydrophobic ILs, namely $Pyr_{14}FSI$, $Pyr_{14}TFSI$, $Pip_{14}TFSI$, and BDMImTFSI ILs. All ILs synthesized with their respective conversions, yields, and impurity contents determined by ionic chromatography are shown in **Table 1**. From the results, the synthesis in the planetary ball mill resulted in a large amount (yields ≥ 80 %) of the desired product and high conversion (≥ 99 %). However, significant mass losses (between 6% to 37%) occurred due to washing the hydrophobic ILs with water, especially for $Pyr_{14}FSI$. Nonetheless, the washing procedure was responsible for reducing bromine levels, which is necessary for ILs to reach Br^- contents < 20 ppm. For applications where bromide concentrations between 100 and 200 ppm are not critical, this step can be omitted from the process. The calibration curves and the chromatograms of the ILs before and after washing with deionized water are

View Article Online
DOI: 10.1039/D6MR00004E

shown in **Figures S2–4** and **Figures S5–9**, respectively, and the suppression of the Br peak can be clearly observed in the latter. It is worth mentioning that the impurity content of the mechanochemically prepared ILs is in the same range as commercial ILs (**Table S1**).

Solid-state reactions and diffusion may occur upon contact between solid reactants, and therefore, the role of mechanical energy is more related to the accelerated transport and mixing of the system. Nonetheless, the formation of liquid phases between the contact of solids is more likely to occur when organic molecules are involved.[45–49] Thus, to better understand the role and the need for mechanical energy in the synthesis of the ILs in this work, a control experiment was performed for Pyr_{14}TFSI IL. In the test, the solid precursors of the IL were simply manually mixed. The mixture (~2.35 g, stoichiometric ratio) was prepared and stored inside a glovebox; the glass vial was sealed, and the evolution of the reaction mixture was monitored over one week (Video S1). No reaction was observed during this period, as the powder mixture remained dry, without any sign of the formation of a liquid phase. This observation indicates that the activation energy barrier for the reaction is not overcome at ambient temperature without mechanical input, and that external mechanical energy is therefore required to promote ion exchange and form the ILs. It should be noted, however, that while this result demonstrates that mechanical action is essential to drive the solid-state metathesis reaction and not merely to mix reactant, it does not allow for discrimination between the individual mechanistic contributions – whether the direct absorption of mechanical energy or indirect effects such as local temperature increase, defect formation, or other relaxation pathways.

Table 1. ILs prepared in the planetary ball mill - Si_3N_4 milling set with 18 milling balls (ø = 10 mm), 500 rpm, 240 min.

Entry	Ionic Liquid	Cation[a]	Anion[b]	Conversion[c] [%]	Yield[c] [%]	Br^-[d] [ppm]	Na^+[e] [ppm]
1	Pyr14TfO		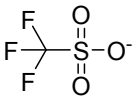	> 99	93.4	68.2	47.70
2	Pyr14TFSI	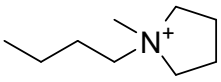	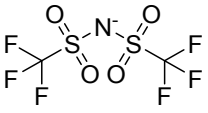	> 99	94.7* 89.4**	172.8 17.9	2.20 < 0.01
3	Pyr14FSI		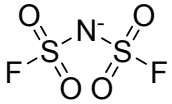	> 99	92.3* 58.1**	147.8 17.9*	2.80 < 0.01
4	Pip14TFSI	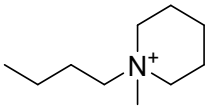	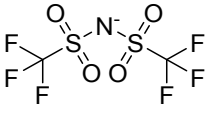	> 99	89.6* 67.1**	141.9 < 10	< 0.01 < 0.01

5	BDMImTFSI	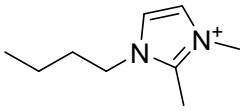	> 99	80.9*	102.5	< 0.01
				74.2**	< 10	< 0.01

[a] from bromides, [b] from sodium salts, [c] mass quantification – details in SI, [d] determined by ionic chromatography, [e] determined by ICP-OES. *Without washing with water, **after washing with water.

PXRD patterns were also acquired for the precipitate obtained from the ball mill synthesis, confirming that only NaBr (a mixture of anhydrous and hydrated forms) remains after 240 min of milling at 500 rpm, as shown in **Figure S10**. No PXRD peaks from the precursors were identified.

The chemical characterization of the final products was performed by ^{1}H and ^{13}C NMR as well as FTIR. In the ^{1}H spectra, no significant variations in proton chemical shifts were observed among the ILs within the Pyr_{14}^{+} series. In the ^{13}C spectra, characteristic signals corresponding to carbon atoms bonded to fluorine in the $TFSI^{-}$ and TfO^{-} anions are clearly observed between 113 and 126 ppm. All chemical shifts are consistent with values previously reported in the literature (**Figures S11–23**).[50–57] ATR-FTIR spectra were recorded for all synthesized ILs (**Figure 4**) and for the anion precursor salts (**Figure S24**). The observed peaks are predominantly assigned to the anions, with bands between 400 and 1600 cm^{-1}, corresponding to SO_3, SO_2, SNS, CS, and CF_3 groups. In addition, symmetric and asymmetric CH_2 stretching modes from the cations are observed in the 3100–2800 cm^{-1} region.[58–64] The most interesting result in the FTIR spectra is that no vibrational bands characteristic of water molecules (3500 cm^{-1} and 1635 cm^{-1}) were observed.[65] Furthermore, before FTIR measurements, the water content was 150–250 ppm by Karl Fischer and dropped to below 10 ppm after drying in the glovebox. It is relevant to note that the presence of water in ILs is detrimental for electrochemical applications, and the results indicate that current approach is able to produce ILs with low water content.

The thermal behavior, stability, and physicochemical properties of ILs are extremely important, which explains why these ionic systems have been widely investigated. TGA measurements were performed to determine the thermal stability of the ILs and their decomposition temperature (T_d), **Figure S25**. According to TGA results, TFSI anion-based ILs exhibit the highest thermal stability amongst the anions studied. In this work, the order of thermal stability is: FSI < TfO < TFSI. Furthermore, DSC measurements of the ILs were carried out to identify the phase transitions that they could exhibit (**Figure S26**). ILs based on the pyrrolidinium cation showed peaks in the DSC curves related to (re)crystallization, solid-solid phase transitions and final melting. From

View Article Online
DOI: 10.1039/D6MR00004E

the DSC curves, it is possible to identify the endothermic melting peaks of the ILs: -15 ºC ($Pyr_{14}TFSI$), - 17 ºC ($Pyr_{14}FSI$), and 6 ºC ($Pyr_{14}TfO$). In addition, exothermic peaks related to (re)crystallization are observed for some of the ILs. Regarding the solid-solid phase transition peaks, $Pyr_{14}TFSI$ shows only one peak (- 27ºC) and $Pyr_{14}FSI$ two peaks (- 45ºC and - 27ºC), one of them at the same position as $Pyr_{14}TFSI$, in agreement with literature data [66]. $Pyr_{14}TfO$ has two solid-solid phase transition peaks (- 36 ºC and - 26 ºC) and a possible (re)crystallization peak at -15 ºC. However, the ILs $Pip_{14}TFSI$ and BDMImTFSI did not show any peaks in the temperature range analyzed owing to the difficulty of crystallization upon cooling, which is expected according to other reports.[55,66–71]

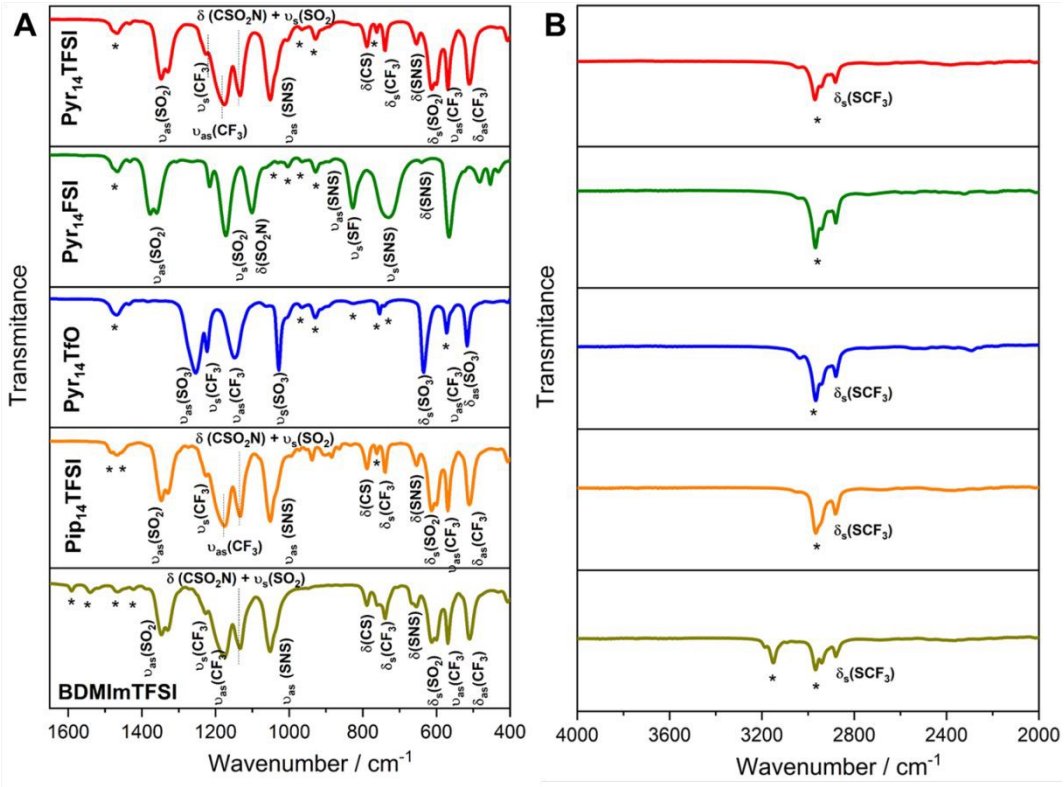

Figure 4. ATR-FTIR spectra of ILs: (A) 400-1600 cm^{-1} and (B) 2000-4000 cm^{-1}.

To assess and compare the mechanochemically prepared ILs, it is essential to evaluate their physicochemical properties in detail and benchmark them against standard commercially available ionic liquids. The physicochemical properties of the ILs were investigated in terms of ionic conductivity, viscosity, and density at different temperatures. The experimental data are summarized in **Tables S2–6**. The temperature dependence of ionic conductivity and viscosity is shown in **Figure S27**. As expected, an increase in temperature results in higher ionic conductivity and lower dynamic viscosity. Among the ILs studied, $Pyr_{14}FSI$ exhibited the highest ionic conductivity and the lowest viscosity, whereas $Pip_{14}TFSI$ showed the lowest conductivity and the highest viscosity.

View Article Online
DOI: 10.1039/D6MR00004E

This behaviour is attributed to differences in ion size, which directly influence ionic mobility and ion-ion interaction.[72] The experimental data for conductivity and viscosity as functions of temperature were fitted using the Vogel–Tammann–Fulcher (VTF) model (**Tables S7–8**), which is widely employed for describing the behaviour of ILs.[55,56,73.] The VTF model demonstrated excellent agreement with the experimental data, capturing the temperature-dependent behavior observed for both ILs.

The temperature dependence of the density of the synthesized ILs was also examined (**Figure S28**). As expected, all ILs exhibited a linear decrease in density with increasing temperature, consistent with typical thermal expansion behavior. Among the ILs investigated, the one containing the TfO^- anion displayed the lowest density, followed by the IL containing the FSI^- anion. Again, this trend can be attributed to differences in anion size and structural flexibility, with TfO^- being the most compact and $TFSI^-$ the largest and most conformationally flexible anion in the series.[74–77] The density of the ILs was further estimated using the empirical model proposed by Ye and Shreeve. [78] The estimated values are in good agreement with experimental measurements (**Table S9**), with minor deviations attributed to the neglect of ion–ion interactions in the volumetric model. The physicochemical properties of the synthesized ILs (ionic conductivity, viscosity, and density) were compared with those of commercially available $Pyr_{14}TFSI$ and $Pyr_{14}FSI$ (**Figure S29** and **Tables S10–11**). The experimental data reveals a strong similarity between commercial ILs and those synthesized in this work, reinforcing the potential of mechanochemical means to produce ILs of excellent quality.

Finally, it is worth noting that the ILs prepared in this study are of interest for electrochemical applications such as electrolytes in batteries, supercapacitors and electrochemical cells for catalysis. Therefore, apart from the ionic conductivity that was measured, electrochemical stability is another property of extreme importance. Electrochemical stability window (ESW) of the ILs was investigated by linear sweep voltammetry using a three-electrode system with an Ag/AgCl electrode as the reference electrode (**Figure 5**). ESW is defined as the potential range within which the IL does not undergo oxidation or reduction, i.e., it is stable.[79,80] The results show that all ILs exhibit high electrochemical stability over a wide potential range with ESW > 4 V, except for $Pyr_{14}TfO$ (3.6 V). The highest ESWs were obtained for $Pip_{14}TFSI$ (5.0 V) and $Pyr_{14}TFSI$ (4.8 V). As can be seen in **Figure 5**, the order of stability of the ILs at positive potential (i.e. where the oxidation reaction occurs) is: $Pyr_{14}TfO$ (1.6 V) < $Pyr_{14}FSI$ (1.9 V) < BDMImTFSI (2.1 V) < $Pyr_{14}TFSI$ (2.2 V) < $Pip_{14}TFSI$ (2.6 V). This behavior can be attributed to the influence of anion structure and the oxidation characteristics of the ionic pairs.[81–85] The higher the positive potential, the stronger the ion-pair interaction and,

View Article Online
DOI: 10.1039/D6MR00004E

consequently, the lower the energy of the occupied molecular orbital (HOMO), making the oxidation of IL more difficult.[82,86,87] Regarding stability at negative potentials (i.e. where reduction reaction occurs), the electrochemical stability follows the trend: $Pyr_{14}TfO$ (- 2.1 V) < $Pyr_{14}FSI$ (-2.3 V) < BDMImTFSI (- 2.4 V) = $Pip_{14}TFSI$ (- 2.4 V) < $Pyr_{14}TFSI$ (- 2.6 V). This result suggests that the response is governed primarily by the nature of the cation, but with a small contribution from the anion. Furthermore, the results indicate that $TFSI^-$ and FSI^- anions display comparable electrochemical stability, with $TFSI^-$ being slightly more stable due to its greater delocalization of charges.[56,88,89] In contrast, $Pyr_{14}TfO$ displayed the shortest ESW, TfO^- being the least stable anion, which can be explained by the higher energy of its lowest unoccupied molecular orbitals (LUMO) energy – more prone to electron acceptance – smaller size, more compact geometry, and lower charge delocalization relative to other anions. [81,85,90–93] Due to differences in electrode materials, electrochemical cell design, scan rate, and cutoff current, a direct comparison between our experimental data and literature values is not possible. However, comparisons of the ESW between the commercial ILs and those synthesized revealed a high degree of similarity between them, **Figure S30**. **Table 2** summarizes the experimental values of the physicochemical and electrochemical properties, under ambient conditions, for the five ILs synthesized via the mechanochemical route.

Table 2. Physical-chemical and electrochemical properties of ILs at 298 K

Ionic Liquid	σ / mS cm^{-1}	η / mPa s	d / g cm^{-3}	$E_{N\,lim}$ / V	$E_{P\,lim}$ / V	ESW / V
$Pyr_{14}TFSI$	3.90	77.81	1.39	- 2.56	2.25	4.8
$Pyr_{14}FSI$	8.59	53.68	1.31	- 2.32	1.89	4.2
$Pyr_{14}TfO$	2.69	176.65	1.25	- 2.06	1.56	3.6
$Pip_{14}TFSI$	1.61	184.38	1.38	- 2.44	2.59	5.0
BDMImTFSI	3.15	100.36	1.42	- 2.39	2.10	4.5

E_N = negative potential limit and E_P = positive potential limit.

View Article Online
DOI: 10.1039/D6MR00004E

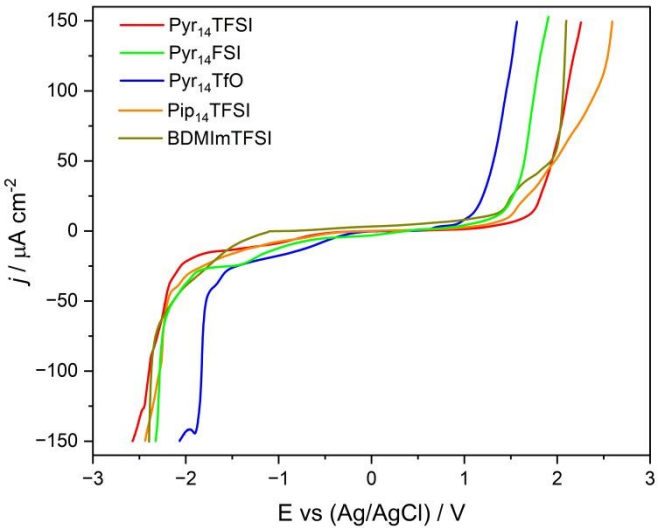

Figure 5. Linear sweep voltammetry of ILs synthesized by the mechanochemical route using a ball mill. Aluminum/carbon as the working electrode and active carbon as the counter electrode. The reference electrode is an Ag/AgCl wire.

Despite the success in preparing the ILs of quality in the planetary mill, as demonstrated by the chemical, physicochemical and electrochemical characterizations, recovering the IL from the milling jar was not straightforward due to the viscous, paste-like character of the sample and the presence of milling balls. The fact that multiple milling bodies are needed in planetary mills, and that as the reaction progresses, more liquid is formed and less volume it occupies in the jar, makes it very difficult to recover the final products directly, as is generally done for solid products. This was one of the reasons a solvent was used in this approach. The mass losses in purification steps, when needed, also encouraged us to pursue another approach that should avoid such IL losses and additional steps. Therefore, based on the high reaction conversions for IL synthesis obtained by milling, we then chose to test other mechanical mixing approaches for both solvent use reduction (or total avoidance) at the same time as scale-up was investigated (**Figure 1B-bottom**). To this end, we used a planetary multi-shaft mixer. Avoiding milling bodies is already a strategy used in the mechanochemical community when using resonant acoustic mixing (RAM).[94,95]

A 99 g scale synthesis of $Pyr_{14}TFSI$ (**Figure 6**) was then performed in a 500 mL stainless-steel planetary mixing vessel equipped with a dual-shaft ribbon-type planetary stirring paddle and an additional single-shaft blade-type stirring paddle operating at 500 rpm (**Figure S31**). The geometry of the stirring systems and rotation speed can generate sufficient shear to induce reaction in such a soft system and ensure a more homogeneous mixing. The synthesis was performed with approximately 99 g of the

View Article Online
DOI: 10.1039/D6MR00004E

reagents, in equimolar amounts, for up to 360 min, with short pauses every 30 min to collect small samples and monitor the reaction progress (**Video S2**). In this case, the separation of solid NaBr products from the IL samples was performed solely by centrifugation. Only the final product (at 360 min) also underwent further work-up, following the same procedure used for the ball mill samples prior to further characterization, so we could compare its physicochemical properties. After only 30 minutes of mixing, the conversion reached 97.2%. Any additional time only increased the conversions slightly, reaching a quantitative conversion after 360 min, with a final isolated yield of 88.4%. PXRD patterns of the precipitate as a function of the mixing time confirm the presence of NaBr only, suggesting an excellent reaction conversion from 30 min (**Figure S32**). The ^{1}H and ^{13}C NMR spectra confirm the formation of IL (**Figures S33 – 36**). Furthermore, ion chromatography results indicated minimal differences in Br^- content between the IL obtained by centrifugation only and that obtained after purification steps such as water washing, with values ranging from 26 – 41 ppm (**Table S12**), indicating that centrifugation might be enough to reach the target purity level.

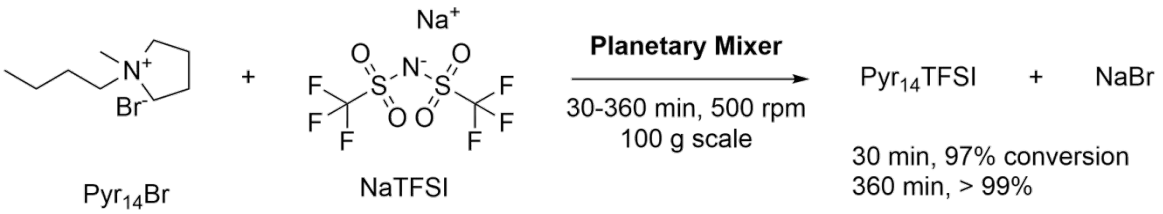

Figure 6. Synthesis of $Pyr_{14}TFSI$ in 100 g scale using a planetary mixer.

To assess the environmental impact of the mechanochemical synthesis, the green metric E-factor (**Table 3**) was estimated. This widely used parameter measures the amount of waste generated in a synthesis or process in mechanochemistry.[96,97] Its ideal value is zero: lower values mean less waste, while higher values indicate a less environmentally friendly process according to green chemistry principles. The equations used are provided in SI (methods). For a more realistic evaluation, first, the simple E-factor (sEF) was calculated, which excludes solvents and water. In this study, it reflects only the synthesis step, without work-up steps. The results showed values close to 1 for all ionic liquids (ILs), which is typical for solvent-free solid-state mechanochemical synthesis.[97]

Table 3. Estimated E-factor metrics for mechanochemical synthesis.

IL	m_R / g	m_S / g	m_W / g	m_{IL} / g	V_S:m_{IL} / mL g^{-1}	sEF	EF	cEF
$Pyr_{14}TFSI$	4.7	26.4	199.4	3.6	5.5	0.3	7.7	63.4
$Pyr_{14}FSI$	3.8	26.4	199.4	2.9	6.8	0.3	9.5	78.7
$Pyr_{14}TfO$	4.3	26.4	-	4.0	5.0	0.1	6.7	-

View Article Online
DOI: 10.1039/D5MR00004E

$Pip_{14}TFSI$	4.5	26.4	199.4	2.5	8.0	0.9	11.6	93.0
BDMImTFSI	4.6	26.4	199.4	2.8	7.1	0.7	10.3	82.8
$Pyr_{14}TFSI$*	99.3	66.0	199.4	83.6	0.6	0.2	1.0	3.4
$Pyr_{14}TFSI$**	99.3	-	-	83.6	-	0.2	0.2	0.2

m_R = mass of reagents; m_S = mass of solvent; m_W = mass of water; m_{IL} = average mass of IL (desired product); V_s = solvent volume (dichloromethane)
Scale-up: * washing + filtration; ** centrifugation only (estimated value).

The E-factor was also estimated, in this case, including the solvent (dichloromethane) used to separate the ILs from NaBr. When the solvent mass is included, the E-factor increases significantly compared to sEF, reaching values between 63 and 93, since the solvent is counted as waste. However, this value could be reduced because the solvent could be easily recovered by adjusting the rotary evaporation conditions. In addition, NaBr can also be recovered due to its high purity, as confirmed by PXRD. Finally, the complete E-factor (cEF), which includes both solvent and water, was estimated. This metric is more appropriate when water is considered, although water is often excluded to avoid artificially high values in the EF metric. As expected, the cEF values are much higher than sEF and EF, especially for ball-milling processes. However, upon scale-up and changing the mechanochemical setup, the value decreases significantly – from 63.4 to 3.4 for the synthesis of $Pyr_{14}TFSI$. If only the centrifugation process is used for separation of IL and NaBr, E-factors reach values as low as 0.2. This result highlights that mechanochemical synthesis, particularly by mechanical mixing and using centrifugation for separation, can be a sustainable approach.

The comparative analysis between the ball milling (lab scale) and the planetary mixer (scale-up) approaches for the mechanochemical synthesis of $Pyr_{14}TFSI$ reveals a fine balance between mechanochemical efficiency and overall process sustainability, **Table S13**. While both approaches achieve high conversions (>99%) and comparable yields (~ 89%), significant differences emerge when considering process intensification, resource consumption, and environmental impact. Although the total processing time reported for the planetary mixer is longer (360 min vs. 240 min for ball milling), the reaction already reached 97% conversion after only 30 min, with the additional time applied to ensure quantitative conversion prior to product recovery. Ball milling affords lower residual bromide content (17.9 ppm vs. 38.2 ppm), suggesting a slightly higher product purity with respect to halide impurities. However, these advantages are offset by significantly higher consumption of solvent and, more critically, water during the purification step – 55.6 mL $g_{product}^{-1}$ for ball milling compared to only 2.4 mL $g_{product}^{-1}$ for the mixer. In contrast, the mixer-based scale-up demonstrates a remarkable reduction in waste generation and auxiliary inputs, reflecting more efficient downstream processing and improved product recovery, and better alignment with the green chemistry principles.

View Article Online
DOI: 10.1039/D6MR00004E

This is clearly reflected in the E-factor values for the synthesis of PyrTFSI for example (Table 3), with the centrifugation-only mixer route achieving cEF as low as 0.2, compared to 63.4 for ball-mill route. Therefore, despite the slightly longer reaction time for quantitative conversion and increased halide residue (but acceptable for several applications), the mixer approach proves to be more sustainable and industrially relevant, as it minimizes resource use and waste generation while maintaining high chemical efficiency. Overall, these results highlight that, although ball milling is highly effective at the laboratory scale, its apparent advantages may be reduced when evaluated from a broader green chemistry perspective, whereas planetary mixer-based approach offers a more viable pathway for scale-up implementation. It is worth mentioning that the use of CH_2Cl_2 in the small-scale work-up, while effective, remains a limitation. Halogen-free solvents with suitable physicochemical properties for IL recovery, combining high volatility, low viscosity, and miscibility with IL products but not with sodium bromide, such as acetone, can be an alternative.

To sum up, the results indicate that mechanical energy within the planetary mixer achieves a higher reaction rate than in the ball mill, which can be attributed to the superior efficiency of mixing in the former. During the reaction, the progressive formation of a liquid phase decreases the efficiency of high-energy impacts during milling, which is typically required for solid–solid systems. In a more fluid regime, shear and bulk mixing become the dominant mechanisms for energy transfer. The continuous shear fields generated in the planetary mixer remain effective even as the mixture becomes fluid, leading to high conversions (30 min, 97%) and facilitated product recovery and work-up.

Conclusions

Overall, the results demonstrate that mechanochemical synthesis is a reliable and scalable approach for producing ILs with fewer steps than the traditional method. This study successfully demonstrated the synthesis of five well-known ILs through the use of mechanochemical approaches to induce ion-exchange (metathesis) reactions and IL formation. Both hydrophobic and, notably, hydrophilic ILs could be prepared in good to excellent yields. It is worth highlighting that for the hydrophilic IL, there was no need to use transition metal sources (often intended to facilitate separation, as in the case of Ag^+ precursors), because no water was used in the synthesis. This, in turn, reduces both the cost of the precursors and the final IL. To the best of our knowledge, the application of a mechanochemical route for the synthesis of ILs with such electrochemical properties has not been previously reported, representing a significant advancement toward solvent-free, low-cost, and time-efficient production of both hydrophilic and hydrophobic ILs. The synthesized ILs displayed excellent quality and physicochemical properties compared to

View Article Online
DOI: 10.1039/D6MR00004E

their benchmark counterparts. More importantly, the scaled-up synthesis provided a straightforward work-up by simple centrifugation, minimizing solvents, purification steps, and reaction time. Given the simplicity of the method based on greater efficiency of mechanical mixing for fluid systems, and the versatility of ion-exchange chemistry, it can be extended to a wide range of ionic systems, including other pyrrolidinium, imidazolium, ammonium, and phosphonium salts. The approach is expected to benefit large-scale preparation of ILs for electrochemical applications where purity, sustainability, and cost reduction are essential.

Authors Contributions

FM: Writing - original draft, Methodology, Validation, Formal analysis. RMT: Conceptualization, Investigation, Funding acquisition, Validation, Data curation, Supervision, Resources, Writing - review & editing. PFMO: Investigation, Funding acquisition, Methodology, Validation, Visualization, Writing - review & editing, Formal analysis, Project administration, Data curation, Supervision, Resources, Conceptualization.

Conflicts of interest

There are no conflicts to declare.

Data Availability

The data supporting this article have been included as part of the Supplementary Information.

Acknowledgements

We thank São Paulo Research Foundation - FAPESP (Grants 2020/14955-6 and 2021/00675-4) for funding. FM also acknowledges CNPq (Grant 141349/2023-9) and FAPESP (Grant 2023/17652-2). We thank the Laboratory of Molecular Spectroscopy (LEM/IQ-USP) for access to the ATR-FTIR equipment.

AI-based tools were used for grammar check and English polishing. No AI tools were used to generate original sentences, paragraphs, scientific content, or images.

References

1 V. H. Paschoal, L. F. O. Faria and M. C. C. Ribeiro, *Chem. Rev.*, 2017, **117**, 7053–7112.

2 Z. Lei, C. Dai, J. Hallett and M. Shiflett, *Chem. Rev.*, 2024, **124**, 7533–7535.

3 T. Welton, *Biophys. Rev.*, 2018, **10**, 691–706.

4 P. Sharma, S. Sharma and H. Kumar, *J. Mol. Liq.*, 2024, **393**, 123447.

5 K. Ueno, H. Tokuda and M. Watanabe, *Phys. Chem. Chem. Phys.*, 2010, **12**, 1649–1658.

6 V. L. Martins and R. M. Torresi, *Curr. Opin. Electrochem.*, 2018, **9**, 26–32.

7 L. S. Domingues, H. G. de Melo and V. L. Martins, *Phys. Chem. Chem. Phys.*, 2023, **25**, 12650–12667.

8 S. K. Singh and A. W. Savoy, *J. Mol. Liq.*, 2020, **297**, 112038.

9 D. R. MacFarlane, N. Tachikawa, M. Forsyth, J. M. Pringle, P. C. Howlett, G. D. Elliott, J. H. Davis, M. Watanabe, P. Simon and C. A. Angell, *Energy Environ. Sci.*, 2014, **7**, 232–250.

10 K. Matuszek, S. L. Piper, A. Brzęczek-Szafran, B. Roy, S. Saher, J. M. Pringle and D. R. MacFarlane, *Adv. Mater., 2024, **36**, 2313023*.

11 L. Miao, Z. Song, D. Zhu, L. Li, L. Gan and M. Liu, *Energy Fuels*, 2021, **35**, 8443–8455.

12 L. Yu and G. Z. Chen, *Front. Chem., 201, **2**, 272-287*.

13 G. Kaur, H. Kumar and M. Singla, *J. Mol. Liq.*, 2022, **351**, 118556.

14 K. Sood, Y. Saini and K. K. Thakur, *Mater. Today Proc.*, 2023, **81**, 739–744.

15 I. Ahmad, B. Elya, Y.I. Ismail, A. Noviani, H. Kuncoro and N.S.S. Ambarwati, *J. Appl. Pharm. Sci.*, 2020, **10**, 1–7.

16 P. V. Barbará, H. Choudhary, P. S. Nakasu, A. Al-Ghatta, Y. Han, C. Hopson, R. I. Aravena, D. K. Mishra, A. Ovejero-Pérez, B. A. Simmons and J. P. Hallett, *Chem. Rev.*, 2025, **125**, 5461–5583.

17 J. L. Shamshina and R. D. Rogers, *Chem. Rev.*, 2023, **123**, 11894–11953.

18 X. Li, K. Chen, R. Guo and Z. Wei, *Chem. Rev.*, 2023, **123**, 10432–10467.

19 G. Li, K. Chen, Z. Lei and Z. Wei, *Chem. Rev.*, 2023, **123**, 10258–10301.

20 G. B. Appetecchi, S. Scaccia, C. Tizzani, F. Alessandrini and S. Passerini, *J. Electrochem. Soc.*, 2006, **153**, A1685.

21 S. Pohlmann and A. Balducci, *Electrochim. Acta*, 2013, **110**, 221–227.

22 S. Jiang, Y. Hu, Y. Wang and X. Wang, *J. Phys. Chem. Ref. Data*, 2019, **48**, 033101.

23 K. R. Seddon, A. Stark and M.-J. Torres, *Pure Appl. Chem.*, 2000, **72**, 2275–2287.

24 V. S. Protsenko, A. A. Kityk, D. A. Shaiderov and F. I. Danilov, *J. Mol. Liq.*, 2015, **212**, 716–722.

25 R. Aranowski, I. Cichowska-Kopczyńska, B. Dębski and P. Jasiński, *J. Mol. Liq.*, 2016, **221**, 541–546.

26 M. L. Williams, S. P. Holahan, M. E. McCorkill, J. S. Dickmann and E. Kiran, *Thermochim. Acta*, 2018, **669**, 126–139.

27 C. J. Clarke, H. Baaqel, R. P. Matthews, Y. Chen, K. R. J. Lovelock, J. P. Hallett and P. Licence, *Green Chem.*, 2022, **24**, 5800–5812.

28 S. Doblinger, T. J. Donati and D. S. Silvester, *J. Phys. Chem. C*, 2020, **124**, 20309–20319.

29 Z. Chen, Z. Li, X. Ma, P. Long, Y. Zhou, L. Xu and S. Zhang, *Green Chem.*, 2017, **19**, 1303–1307.

30 M. Sakhalkar, P. Aduri, S. Lande and S. Chandra, *Clean Technol. Environ. Policy*, 2020, **22**, 59–71.

31 A. Aljuhani, W. S. El-Sayed, P. K. Sahu, N. Rezki, M. R. Aouad, R. Salghi and M. Messali, *J. Mol. Liq.*, 2018, **249**, 747–753.

32 G. Zbancioc, I. I. Mangalagiu and C. Moldoveanu, *Ultrason. Sonochem.*, 2015, **23**, 376–384.

33 J. Ding and D. W. Armstrong, *Chirality*, 2005, **17**, 281–292.

34 E. Simonetti, M. De Francesco, M. Bellusci, G. Kim, F. Wu, S. Passerini and G. B. Appetecchi, *ChemSusChem*, 2019, **12**, 4946–4952.

35 A. I. Ikeuba, B. E. Usibe, C. U. Sonde, R. C. Anozie, H. O. Edet, O. E. Obono and B. I. Ita, *Chem. Africa*, 2024, **7**, 3531–3548.

36 A. J. Greer, J. Jacquemin and C. Hardacre, *Molecules*, 2020, **25**, 5207.

37 P. F. M. de Oliveira, R. M. Torresi, F. Emmerling and P. H. C. Camargo, *J. Mater. Chem. A*, 2020, **8**, 16114–16141.

38 J.-L. Do and T. Friščić, *ACS Cent. Sci.*, 2017, **3**, 13–19.

39 J. L. Howard, Q. Cao and D. L. Browne, *Chem. Sci.*, 2018, **9**, 3080–3094.

40 V. Martinez, T. Stolar, B. Karadeniz, I. Brekalo and K. Užarević, *Nat. Rev. Chem.*, 2022, **7**, 51–65.

41 A. P. Amrute, J. De Bellis, M. Felderhoff and F. Schüth, *Chem. Eur. J.*, 2021, **27**, 6819–6847.

42 N. R. Rightmire and T. P. Hanusa, *Dalton Trans.*, 2016, **45**, 2352–2362.

43 B. G. Fiss, A. J. Richard, G. Douglas, M. Kojic, T. Friščić and A. Moores, *Chem. Soc. Rev.*, 2021, **50**, 8279–8318.

44 I. C. B. Martins, M. C. Oliveira, H. P. Diogo, L. C. Branco and M. T. Duarte, *ChemSusChem*, 2017, **10**, 1360–1363.

45 J. Zotova, Z. Wojnarowska, B. Twamley, M. Paluch and L. Tajber, *ACS Sustain. Chem. Eng.*, 2020, **8**, 18266–18276.

46 O. Dolotko, J. W. Wiench, K. W. Dennis, V. K. Pecharsky and V. P. Balema, *New J. Chem.*, 2010, **34**, 25–28.

47 H. Watanabe, R. Hiraoka and M. Senna, *Tetrahedron Lett.*, 2006, **47**, 4481–4484.

48 K. Chadwick, R. Davey and W. Cross, *CrystEngComm*, 2007, **9**, 732.

49 R. Kuroda, K. Higashiguchi, S. Hasebe and Y. Imai, *CrystEngComm*, 2004, **6**, 463-468.

50 P. B. Webb, M. F. Sellin, T. E. Kunene, S. Williamson, A. M. Z. Slawin and D. J. Cole-Hamilton, *J. Am. Chem. Soc.*, 2003, **125**, 15577–15588.

51 M. Jankowska-Wajda, O. Bartlewicz, P. Pietras and H. Maciejewski, *Catalysts*, 2020, **10**, 919.

52 M. I. Cabaço, M. Besnard, F. V. Chávez, N. Pinaud, P. J. Sebastião, J. A. P. Coutinho and Y. Danten, *J. Chem. Phys.*, 2014, **140**, 244307.

53 M. Zawadzki, M. Królikowska and P. Lipiński, *Thermochim. Acta*, 2014, **589**, 148–157.

54 K. V. Tyutyukin, A. V. Ievlev, V. V. Matveev, L. M. Varela and O. Cabeza, *Appl. Magn. Reson.*, 2024, **55**, 785–794.

55 M. Moreno, M. Montanino, M. Carewska, G. B. Appetecchi, S. Jeremias and S. Passerini, *Electrochim. Acta*, 2013, **99**, 108–116.

56 N. Sánchez-Ramírez, B. D. Assresahegn, D. Bélanger and R. M. Torresi, *J. Chem. Eng. Data*, 2017, **62**, 3437–3444.

57 A. R. Neale, C. Schütter, P. Wilde, P. Goodrich, C. Hardacre, S. Passerini, A. Balducci and J. Jacquemin, *J. Chem. Eng. Data*, 2017, **62**, 376–390.

58 O. B. Babushkina, *Z. Naturforsch. A*, 2008, **63**, 66–72.

59 D. Kumar and S. A. Hashmi, *Solid State Ion.*, 2010, **181**, 416–423.

60 W. Zou, J. Zhang, M. Liu, J. Li, Z. Ren, W. Zhao, Y. Zhang, Y. Shen and Y. Tang, *Adv. Mater,* 2024, **36**, 2400537.

61 L. Schafzahl, I. Hanzu, M. Wilkening and S. A. Freunberger, *ChemSusChem*, 2017, **10**, 401–408.

62 R. Chen, Y. Chen, L. Zhu, Q. Zhu, F. Wu and L. Li, *J. Mater. Chem. A Mater.*, 2015, **3**, 6366–6372.

63 D. H. Johnston and D. F. Shriver, *Inorg. Chem.*, 1993, **32**, 1045–1047.

64 S. Khurana and A. Chandra, *J. Polym. Sci. B Polym. Phys.*, 2018, **56**, 207–218.

65 B. L. Mojet, S. D. Ebbesen and L. Lefferts, *Chem. Soc. Rev.*, 2010, **39**, 4643-4655.

66 M. Kunze, S. Jeong, E. Paillard, M. Winter and S. Passerini, *J. Phys. Chem. C*, 2010, **114**, 12364–12369.

67 E. Gómez, N. Calvar, Á. Domínguez and E. A. Macedo, *Fluid Phase Equilib.*, 2018, **470**, 51–59.

68 R. Lin, P.-L. Taberna, S. Fantini, V. Presser, C. R. Pérez, F. Malbosc, N. L. Rupesinghe, K. B. K. Teo, Y. Gogotsi and P. Simon, *J. Phys. Chem. Lett.*, 2011, **2**, 2396–2401.

69 P. Raut, S. Yuan, T. Miyoshi and S. C. Jana, *Polymer.*, 2020, **211**, 123081.

70 M. Montanino, M. Carewska, F. Alessandrini, S. Passerini and G. B. Appetecchi, *Electrochim. Acta*, 2011, **57**, 153–159.

71 A. V. Agafonov, L. M. Ramenskaya, E. P. Grishina and N. O. Kudryakova, *RSC Adv.*, 2021, **11**, 38605–38615.

72 S. Tsuzuki, H. Tokuda, K. Hayamizu and M. Watanabe, *J. Phys. Chem. B*, 2005, **109**, 16474–16481.

73 V. L. Martins, N. Sanchez-Ramirez, M. C. C. Ribeiro and R. M. Torresi, *Phys. Chem. Chem. Phys.*, 2015, **17**, 23041–23051.

74 K. S. Han, J. Chen, R. Cao, N. N. Rajput, V. Murugesan, L. Shi, H. Pan, J.-G. Zhang, J. Liu, K. A. Persson and K. T. Mueller, *Chem. Mater.*, 2017, **29**, 9023–9029.

75 A. Martinelli, A. Matic, P. Johansson, P. Jacobsson, L. Börjesson, A. Fernicola, S. Panero, B. Scrosati and H. Ohno, *J. Raman Spectrosc.*, 2011, **42**, 522–528.

76 R. Yunis, G. M. A. Girard, X. Wang, H. Zhu, A. J. Bhattacharyya, P. Howlett, D. R. MacFarlane and M. Forsyth, *Solid State Ion.*, 2018, **327**, 83–92.

77 M. Brinkkötter, E. I. Lozinskaya, D. O. Ponkratov, P. S. Vlasov, M. P. Rosenwinkel, I. A. Malyshkina, Y. Vygodskii, A. S. Shaplov and M. Schönhoff, *Electrochim. Acta*, 2017, **237**, 237–247.

78 C. Ye and J. M. Shreeve, *J. Phys. Chem. A*, 2007, **111**, 1456–1461.

79 M. Chen, J. Zhang, X. Ji, J. Fu and G. Feng, *Curr. Opin. Electrochem.*, 2022, **34**, 101030.

80 Y.-H. Tian, G. S. Goff, W. H. Runde and E. R. Batista, *J. Phys. Chem. B*, 2012, **116**, 11943–11952.

81 Y. Chen, S. Liu, Z. Bi, Z. Li, F. Zhou, R. Shi and T. Mu, *Green Energy Environ.*, 2024, **9**, 966–991.

82 N. De Vos, C. Maton and C. V. Stevens, *ChemElectroChem*, 2014, **1**, 1258–1270.

83 T. P. D. De Silva, G. Sahasrabudhe, B. Yang, C.-H. Wang, P. K. Chhotaray, E. E. Nesterov and I. M. Warner, *J. Phys. Chem. A*, 2019, **123**, 111–119.

84 N. Shida, Y. Imada, S. Nagahara, Y. Okada and K. Chiba, *Commun. Chem.*, 2019, **2**, 24.

85 F. Wang and J. Cheng, *Chem. Sci.*, 2022, **13**, 11570–11576.

86 J. M. Kahk, I. Kuusik, V. Kisand, K. R. J. Lovelock and J. Lischner, *NPJ Comput. Mater.*, 2020, **6**, 148.

87 A. Paolone, S. Di Muzio, O. Palumbo and S. Brutti, *Entropy*, 2023, **25**, 793.

88 K. C. Lethesh, A. Bahaa, M. Abdullah, M. O. Bamgbopa and R. A. Susantyoko, *Front. Chem.*, 2022, **10**, 859304.

89 H. Zhang, X. Cheng, Q. Ma, W. Feng, L. Zheng, J. Nie, X. Huang, M. Armand and Z. Zhou, *Electrochim. Acta*, 2016, **207**, 66–75.

View Article Online
DOI: 10.1039/D6MR00004E

90 M. Watanabe, M. L. Thomas, S. Zhang, K. Ueno, T. Yasuda and K. Dokko, *Chem. Rev.*, 2017, **117**, 7190–7239.

91 A. Paolone and S. Brutti, *Materials*, 2021, **14**, 3221.

92 C. Kang, J. Zhu, Y. Wang, S. Ye, Y. Xiong, F. Kong and G. Yin, *Energy Storage Mater.*, 2023, **61**, 102898.

93 Y. Dong, L. Miao, G. Ma, S. Di, Y. Wang, L. Wang, J. Xu and N. Zhang, *Chem. Sci.*, 2021, **12**, 5843–5852.

94 A. A. L. Michalchuk and E. V. Boldyreva, in *Encyclopedia of Green Chemistry*, Elsevier, 2025, pp. 532–541.

95 A. A. L. Michalchuk, K. S. Hope, S. R. Kennedy, M. V. Blanco, E. V. Boldyreva and C. R. Pulham, *Chem. Commun.*, 2018, **54**, 4033–4036.

96 N. Fantozzi, J.-N. Volle, A. Porcheddu, D. Virieux, F. García and E. Colacino, *Chem. Soc. Rev.*, 2023, **52**, 6680–6714.

97 R. A. Sheldon, *Green Chem.*, 2023, **25**, 1704–1728.

Data Availability

View Article Online
DOI: 10.1039/D6MR00004E

The data supporting this article have been included as part of the Supplementary Information.

Sincerely,

Dr. Paulo Filho Marques de Oliveira, Assist Prof.
Instituto de Química - Universidade de São Paulo
B05, Sala 554
Av Prof. Lineu Prestes, 748 - Vila Universitária
05508-000, São Paulo - SP – Brasil.